Present-day motion of the Arabian plate

Renier Viltres, Sigurjón Jónsson, Abdulaziz Alothman, Shaozhuo Liu, Sylvie Leroy, Frédéric Masson, Cécile Doubre, Robert Reilinger

Present-day motion of the Arabian plate

Renier Viltres[1], Sigurjón Jónsson[1], Abdulaziz O. Alothman[2], Shaozhuo Liu[1], Sylvie Leroy[3], Frédéric Masson[4], Cécile Doubre[4]and Robert Reilinger[5]

[1]King Abdullah University of Science and Technology (KAUST), Physical Science and Engineering Division, Thuwal 23955-6900, Saudi Arabia
[2]King Abdulaziz City for Science and Technology (KACST), Space and Aeronautics Institute, Geodesy and Navigation Center, Riyadh 11442, Saudi Arabia
[3]Sorbonne Université, INSU, CNRS, ISTeP, Paris, France
[4]Institut de Physique du Globe de Strasbourg, UMR 7516, Universite de Strasbourg/EOST, CNRS, 5 rue Rene Descartes, F-67084 Strasbourg Cedex, France
[5]Department of Earth, Atmospheric, and Planetary Sciences, Massachusetts Institute of Technology, Cambridge, Massachusetts, USA

Corresponding author: Renier Viltres, renier.ladrondeguevara@kaust.edu.sa

Abstract

The present-day motions in and around the Arabian plate involve a broad spectrum of tectonic processes including plate subduction, continental collision, seafloor spreading, intraplate magmatism, and continental transform faulting. Therefore, good constraints on the relative plate rates and directions, and on possible intraplate deformation, are crucial to assess the seismic hazard at the boundaries of the Arabian plate and areas within it. Here we combine GNSS-derived velocities from 168 stations located on the Arabian plate with a regional kinematic block model to provide updated estimates of the present-day motion and internal deformation of the plate. A single Euler pole at 50.93±0.15°N, 353.91±0.25°E with a rotation rate of 0.524±0.001°/Ma explains well almost all the GNSS station velocities relative to the ITRF14 reference frame, confirming the large-scale rigidity of the plate. Internal strain rates at the plate-wide scale (~0.4 nanostrain/yr) fall within the limits for stable plate interiors, indicating that differential motions are compensated for internally, which further supports the coherent rigid motion of the Arabian plate at present. At a smaller scale, however, we identified several areas within the plate that accommodate strain rates of up to ~8 nanostrain/yr. Anthropogenic activity and possible subsurface magmatic activity near the western margin of the Arabian plate are likely responsible for the observed local internal deformation. Put together, our results show a remarkable level of stability for the Arabian lithosphere, which can withstand the long-term load forces associated with active continental collision in the northeast and breakup to the southwest with minimal internal deformation.

Plain Language Summary

Good knowledge of relative motions between tectonic plates is crucial for earthquake hazard assessments. In this study, we use new geodetic GNSS (also known as GPS) measurements from many stations on the Arabian Peninsula to provide updated information about the motion of the Arabian plate relative to its neighboring tectonic plates. The new GNSS velocities indicate that as a whole, the Arabian plate moves like a single block, resisting well the push and pull forces associated with plate boundary processes at its margins. However, when looking at smaller scales, several areas within the plate are deforming, with aquifer pressure changes due to groundwater pumping being the main cause of the deformation in most cases.

1 Introduction

The Arabian plate began its independent motion in the late Oligocene, likely facilitated by extensional forces associated with plume-related volcanism beneath the African lithosphere and northward subduction of the Neo-Tethys ocean in response to the Indian-Eurasian continental collision (McClusky et al., 2003; Bellahsen et al., 2003; Bosworth et al., 2005; Fournier et al., 2010). The location of the plate boundaries, as we know them today, resulted from several phases of structural reorganization taking place since the early Miocene including: 1) simultaneous rifting along the Red Sea and Gulf of Aden at ~25 Ma, 2) seafloor spreading in the Gulf of Aden and the Red Sea since ~17.6 Ma and ~13 Ma, respectively, 3) continental collision along the Bitlis suture and the Bitlis-Zagros fold and thrust belt since ~14 Ma, 4) connection of the northern Red Sea with the East-Anatolian fault through the Dead Sea transform fault at ~14 Ma, 5) formation and isolation of microplates including the Danakil and Sinai (~13 Ma) blocks, 6) stabilization of the southernmost Red Sea and full transfer of the Nubian-Arabian extension west of the Danakil block ~8-5 Ma, and 7) formation of the ~800 km long Owen Fracture Zone (OFZ) connecting the Aden-Owen-Carlsberg triple junction to the Makran subduction zone at ~2.4-6 Ma (Vernant et al., 2004; Bosworth et al., 2005; Garfunkel & Beyth, 2006; Fournier et al., 2008; McClusky et al., 2010; Fournier et al., 2010; Reilinger & McClusky, 2011; Leroy et al., 2012; Robinet et al., 2013; Reilinger et al., 2015; Varet, 2018b; Bosworth et al., 2019; Rodriguez et al., 2019; Gomez et al., 2020; Augustin et al., 2021, and references therein, Fig. 1).

Subduction of Nubian and Arabian oceanic lithosphere beneath Eurasia continues at present and is the main driver of the observed oblique opening along the Red Sea and Gulf of Aden rifts, right-lateral strike-slip motion along the OFZ, frontal shortening along the Makran subduction zone, transpression along the Bitlis-Zagros fold and thrust belt, and predominantly left-lateral strike-slip motion along the Dead Sea and East Anatolian faults (Vernant et al., 2004; Reilinger et al., 2006; ArRajehi et al., 2010; Rodriguez et al., 2019; Hamiel & Piatibratova, 2019; Gomez et al., 2020, Fig. 1). Earlier studies combining GNSS measurements, magnetic anomaly profiles, earthquake slip vectors and plate paleo-positions indicate that the relative motions involving the Arabian-Nubian, Arabian-Somalian, and Arabian-Eurasian plate pairs have been unchanged since at least 11, 15, and 24 Ma, respectively (Chu & Gordon, 1998; McQuarrie et al., 2003; ArRajehi et al., 2010; Fournier et al., 2010; Iaffaldano et al., 2014; Schettino et al., 2016). Nevertheless, temporal variations in the Arabian-Nubian-Eurasian relative motion has been suggested based on GNSS-derived angular velocities from stations in Yemen, Bahrain, Oman, and Iran, finite rotations of the ocean-floor along the Eurasia-Nubia-North America plate circuit, as well as global dynamic models (e.g., Calais et al., 2003; Austermann & Iaffaldano, 2013). This change in the con-

vergence rate is interpreted to have initiated since ~5-3.2 Ma, coeval with the most recent phase of orogenic uplift within the Zagros and adjacent regions (Austermann & Iaffaldano, 2013).

The Arabian plate interior is composed of two main crustal domains of continental lithosphere, likely resulting from mantle processes and marginal uplift within the Red Sea and the Gulf of Aden (Stern & Johnson, 2010). The eastern part of the plate is dominated by Mesozoic to Cenozoic sedimentary rocks, while the Arabian shield in the west is primarily composed of Precambrian rocks and hosts several Cenozoic alkalic volcanic fields that remain volcanically active (Hancock et al., 1984; Bosworth et al., 2005; Stern & Johnson, 2010, Fig. 1). Intraplate magmatism accounts for several volcanic eruptions over the last few kiloyears and a recent rifting event affecting the western margin of the plate in 2009 (Camp & Roobol, 1989; Pallister et al., 2010; Jónsson, 2012; Xu et al., 2016). The orientation of dyke intrusions, the roughly N-S arrangement of the major volcanic fields (Harrat Rahat, Harrat Khaybar, and Harrat Ithnayn) as well as the linear vent systems marking their central axes all suggests a stress field dominated by E-W to ENE-WSW directed extension on the western margin of the plate (Camp et al., 1992b; Pallister et al., 2010; Trippanera et al., 2019). This present-day state of stress appears to be governed by northward asthenospheric flow starting beneath Afar and running through the southern Red Sea towards the western margins of the plate rather than by Precambrian basement intraplate tectonic structures (Camp & Roobol, 1989; Pallister et al., 2010; Lim et al., 2020).

The main tectonic structures within the plate interior are marked by the Najd fault system, the Central Arabian graben system, the Al-Batin arch, and the Azraq graben (Hancock et al., 1984; Konert et al., 2001; Faqira et al., 2009; Stern & Johnson, 2010, Fig. 1). The Najd fault system strikes NW-SE across the Precambrian shield and is predominantly composed of sinistral strike-slip faults and brittle to brittle-ductile shears zones (Stern & Johnson, 2010). The Central Arabian graben system runs for ~560 km on the central part of the plate and is formed by a series of grabens and troughs trending east towards Qatar in the south, and NW-SE (i.e., subparallel to the terrane boundaries of the Precambrian shield) in the north (Hancock et al., 1984). The NE-trending Al-Batin arch runs across the eastern part of the plate from near the Precambrian shield towards Iran with limited observations suggesting tectonic control by lineaments of NE-trending normal faults (Hancock et al., 1984; Faqira et al.,

2009). The Azraq graben strikes NW and has been interpreted to represent a mechanically weak trend on the northern part of the plate (Konert et al., 2001). Despite the presence of these internal structures, seismic activity is primarily focused along the plate boundaries (ISC, 2022). In addition, intraplate earthquakes, albeit infrequent (i.e., Tabuk 2004, Lunayyir 2009) show relation with tensional stresses associated with the opening of the Red Sea extending several tens of kilometers into the western margin of the plate (Pallister et al., 2010; Aldamegh et al., 2012; Xu et al., 2015b). Furthermore, significant ground subsidence, shallow seismicity, opening cracks, and sinkholes documented in the recent years towards the center of the plate indicate response to groundwater over-exploitation and rapid urbanization (e.g., Othman et al., 2018).

Estimates of the relative motion at the plate boundaries surrounding the Arabian plate, which provide important inputs for regional earthquake hazard assessments, mostly rely on GNSS observations and kinematic block modeling (e.g., Vigny et al., 2006; ArRajehi et al., 2010; Reilinger & McClusky, 2011; Kreemer et al., 2014; Altamimi et al., 2017). However, despite an overall consistency between kinematic models, differences in GNSS site numbers, geographic distribution, and observation time spans have resulted in some discrepancies between the predicted relative motions. Adding to that, the present-day motion and boundary configuration of several microplates surrounding the Arabian plate are still not fully resolved (e.g., Sinai, Carmel, Mt. Lebanon, Syrian Coast, Helmand, Lut, Central Iran, Reilinger et al., 2006; ArRajehi et al., 2010; Gomez et al., 2020, Fig. 1). Furthermore, GNSS-derived differential motions have indicated that the Arabian plate is coherently moving as a single block, although localized strains consistent with shortening in the Palmyride Mountains and extension within the western Arabian margins have been observed (e.g., ArRajehi et al., 2010; Aldaajani et al., 2021). All the studies above, however, relied on a limited number of GNSS stations from within the plate interior or included sites spanning only up to 18 months of measurements, yielding results with limited resolution.

Here we report on the analysis of measurements from 189 GNSS stations spanning up to 17 years of continuous and survey mode observations and provide updated constraints on the present-day motions of the Arabian plate. We re-estimated the angular velocity describing the current Arabian-International Terrestrial Reference Frame 2014 (ITRF14) relative motion using our new GNSS-derived velocities for stations free from plate-boundary effects. Then, we combined our results with similar estimates for the neighboring tectonic plates into a kinematic block model to address the present-day relative motions at the plate boundaries surrounding the Arabian plate. From the same set of GNSS stations, we present a horizontal strain-rate field for the interior of the Arabian plate on a calculation grid of

154 0.5° in latitude and longitude. Finally, we discuss the implications of our new results for
155 the plate's motion during recent geological times, as well as for the possible relation of the
156 estimated internal strains with anthropogenic activity, and subsurface magmatic activity.

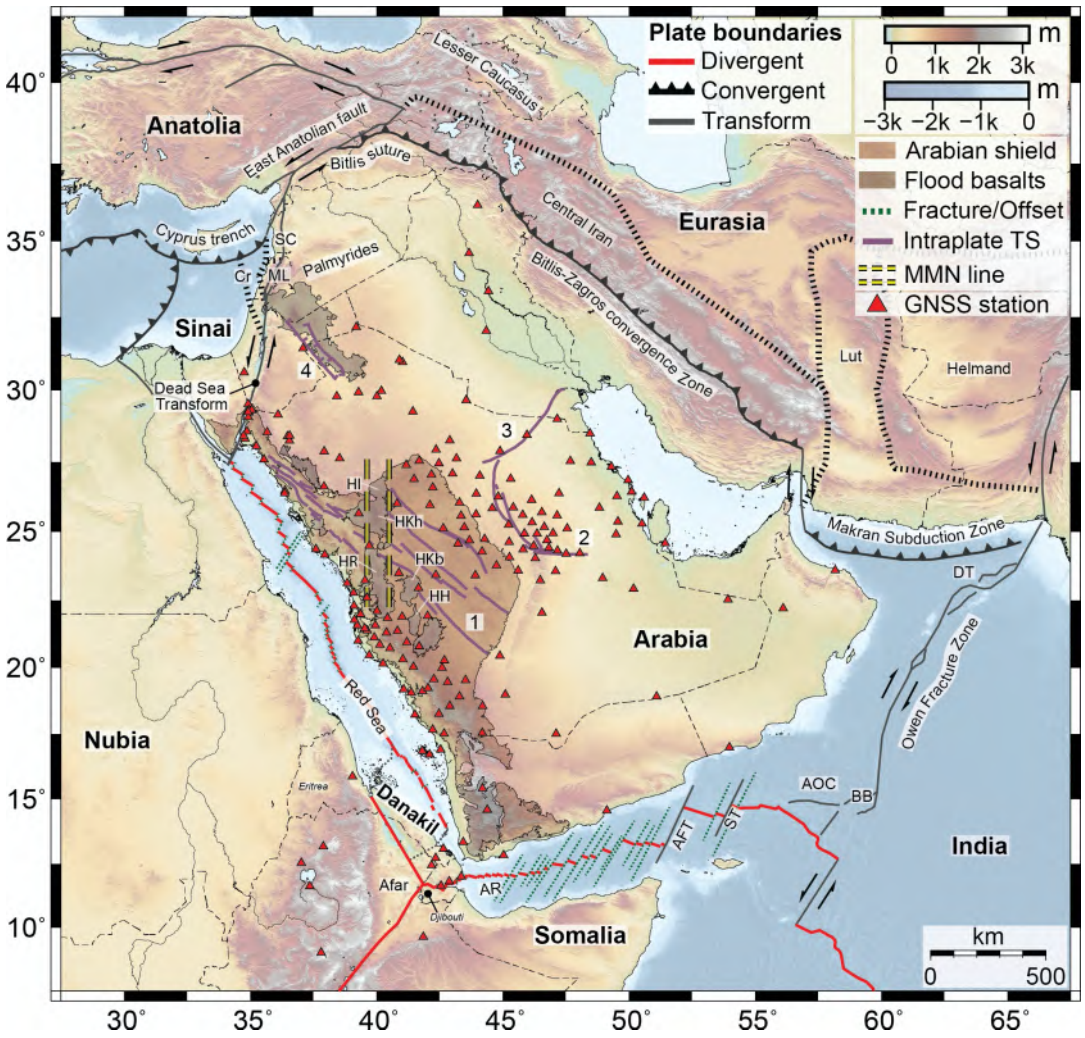

Figure 1. Main plate boundaries around the Arabian plate defined after Bosworth et al. (2005); Schettino et al. (2016); Doubre et al. (2017); Rodriguez et al. (2019); Viltres et al. (2020); Ribot et al. (2021) and A. Afifi (pers. comm.). Background hillshaded topography and bathymetry from `http://topex.ucsd.edu/`. The Carmel (Cr), Mt. Lebanon (ML), Syrian Coast (SC), Central Iran, Lut, and Helmand blocks were drawn after Gomez et al. (2020), Reilinger et al. (2006) and Vernant et al. (2004). Other abbreviations: Tectonic structure (TS), Harrat Rahat (HR), Khaybar (HKh), Ithnayn (HI), Kishb (HKb), Hadan (HH); Alula-Fartak (AFT), Socotra-Hadbeen (ST) transform fault; Aden ridge (AR), Aden-Owen-Carlsberg triple junction (AOC), Dalrymple Trough (DT), Beautemps-Beaupré pull-apart basin (BB), Makkah-Madinah-Nafud (MMN) line. Solid purple lines mark the major intraplate tectonic structures with numbers being 1) Najd fault system, 2) Central Arabian graben system, 3) Al-Batin arch and 4) Azraq graben modified after Hancock et al. (1984), Konert et al. (2001) and Stern and Johnson (2010).

2 Data and Methods

2.1 GNSS datasets and processing

The geodetic data we used for both the Euler pole and the strain-rate tensor estimations are from 189 GNSS stations spanning up to ~17 years of continuous or survey-mode observations (Fig. 1). The longest time-series (>5 years) belong to continuous GNSS stations installed in the area by MIT (data available at `https://www.unavco.org`), King Abdulaziz City for Science and Technology (KACST), and the IGS (data available at `https://cddis.nasa.gov/archive/gnss/data/daily`). Most of the station data (126 stations), however, only span up to 2.5 years, and were provided by the Saudi Arabia General Authority for Survey and Geospatial Information (data available at `https://ksacors.gcs.gov.sa`, see Table S1 of the supplementary material for details). Additional datasets include GNSS observations from East Africa acquired by MIT, King Abdullah University of Science and Technology (KAUST), and the French mobile network (data available at King et al., 2019; Jónsson, 2020, and `https://gpsmob.resif.fr/donnees`, respectively), and three GNSS stations installed in Yemen and Oman during the YOCMAL project (e.g., Leroy, 2013). Observations from a total of 19 IGS fiducial GNSS stations complemented the geodetic dataset and were used for reference frame stabilization.

The GNSS observations were analyzed with the GAMIT/GLOBK GNSS analysis package (Herring et al., 2018), following the processing steps described by Floyd et al. (2010) and Kogan et al. (2012). In the first step, daily loosely constrained station coordinates and their associated covariance matrices (quasi-observations) were obtained from the double-difference GNSS phase observations. In the next step, we used the GLOBK Kalman filter (Herring et al., 2018) to combine daily quasi-observations into position time-series aligned to the ITRF14 reference frame (defined after Altamimi et al., 2017). The daily solution alignment was achieved by estimating a six-parameter Helmert transformation constraining the positions of the 19 fiducial IGS stations to their ITRF14 values. At this step, outliers were removed from the daily position time-series and appropriate weights to the observations were determined. In the final step, the cleaned daily solutions from the survey-mode and continuous observations were combined into a single survey or 7-day position time-series, respectively, to minimize short-term noise effects.

To better constrain the GNSS station's secular motion given that most of the time-series only extend up to 2.5 years, and to take the station-specific noise structure into consideration, we used the HECTOR-v1.7.2 software package (Bos et al., 2013) instead of the GLOBK Kalman filter for the velocities estimation. It allows for automatic offset detection and outlier removal while estimating trajectory model parameters with realistic uncertainties

in time-series with temporally correlated noise (Bos et al., 2008, 2013; Williams, 2003, 2008, and references therein). For each component, we described the temporal variations in the position time-series by a trajectory model composed of a linear trend, annual and semiannual oscillations, and step-function terms to account for earthquakes and/or hardware change. Likewise, the noise within each position time-series was assumed to derive from a linear combination of white and power-law components. For the limited number of survey-mode observations, the trajectory model only included the parameters defining a linear trend to describe the time-series. In addition, we added random walk process noise components that predict the same uncertainties as the median values of the noise structure derived from the continuous GNSS stations prior to the velocity estimation. Finally, angular velocities from the Altamimi et al. (2017) plate motion model were used to rotate the estimated absolute station velocities relative to the Nubian plate (Fig. 2).

2.2 Angular velocity and strain-rate tensor estimation

For the estimation of the Arabian-ITRF14 angular velocity, we constructed a simplified block model based on the plate boundaries shown in Fig. 1 using the TDEFNODE software (McCaffrey, 1995, 2002, 2009, Fig. 2). Then, we used similar estimates for the neighboring tectonic plates to estimate the rates and azimuths of present-day motions at the major plate boundaries in the region (e.g, Red Sea-Afar, Dead Sea Transform Fault, Zagros-Makran collision zone, Owen Fracture Zone, etc., Fig. 1). Since the GNSS observations are mostly from the Arabian plate (Fig. 2), the angular velocities for the major neighboring tectonic plates (Nubian, Eurasian, Indian) were taken from Altamimi et al. (2017) and DeMets et al. (2019), and the microplates (Danakil, Sinai, Anatolian) angular velocities were taken from Viltres et al. (2020), Hamiel and Piatibratova (2019), and Gomez et al. (2020), respectively (see paragraph below for details). Our regional-scale kinematic model considered free-slip along the fault segments defining the block's boundaries, while the Euler vectors (angular velocities) were estimated assuming both (1) rigid block motion, and (2) internal deformation, by including the parameters defining a uniform horizontal strain-rate tensor in the optimization. In both cases, the model parameters were estimated by minimizing the residual horizontal velocities at GNSS sites located at least 50 km away from the prescribed block boundaries by means of the weighted least squares method.

The motion of the Arabian plate was constrained by 168 sites after removing 11 GNSS stations from within 50 km of the plate boundaries and three GNSS sites (HL04, TB06, MK94) with time-series affected by transient signals, and therefore, not representing the steady-state motion of the plate (Table S1). The angular velocities for the Nubian and Eurasian plates were defined after the Altamimi et al. (2017) plate motion model and con-

strained by 24 and 97 sites, respectively. For the Indian and Somalian plates, we used the angular velocities from DeMets et al. (2019). Their estimates include 29 and 11 GNSS sites, respectively, and are better constrained than the estimates in Altamimi et al. (2017), which include only 3 stations on each plate. The motion of the Danakil, Sinai, and Anatolian microplates were constrained by 8 (Viltres et al., 2020), 7 (Hamiel & Piatibratova, 2019), and 11 (Gomez et al., 2020) GNSS stations, respectively.

We estimated the strain-rate tensor and rotation rates for the entire Arabian plate at a spatial resolution of 0.5° using the "strain tensor from inversion of baselines", STIB method (Masson et al., 2014). The STIB method derives from the "inversion of baseline variations" method, developed by Spakman and Nyst (2002), and has been successfully used in regions like Iran, Afar, and the French Alps (e.g., Doubre et al., 2017; Masson et al., 2014; Henrion et al., 2020). It uses relative baseline changes between all possible pairs of GNSS stations within a network to derive the velocity gradient at each computation node, independently of any reference frame (Doubre et al., 2017; Masson et al., 2014). This approach makes the method less dependent on the network geometry and the quality of the velocity field, compared to similar methods like the triangle and the gridded approaches (Wu et al., 2011; Masson et al., 2014; Doubre et al., 2017). Similar to the angular velocity estimation, only GNSS stations at least 50 km away from the prescribed block boundaries were used in the inversion. The inversion was performed without regularization (spatial smoothing), and the covariance matrix for the a priori model was set to be diagonal with a constant value of $10^{-9}yr^{-1}$, i.e., of the order of magnitude of the expected internal deformation within the plate (e.g., Vigny et al., 2006).

3 Results

3.1 GNSS velocity field

The GNSS station velocities show a consistent northeast motion and rotation of the Arabian plate, relative to the Nubian plate (Fig. 2). The motion is ~19 mm/yr towards ~N51°E in the southernmost Red Sea, ~12 mm/yr towards ~N40°E at ~21.5°N, and ~7 mm/yr towards ~N23°E in the Gulf of Aqaba area (Fig. 2). The horizontal velocity uncertainties for GNSS stations within the Arabian plate interior (>50 km from plate boundary) average to 0.42 mm/yr, and reach up to 1.13 and 1.35 mm/yr for the north and east component, respectively.

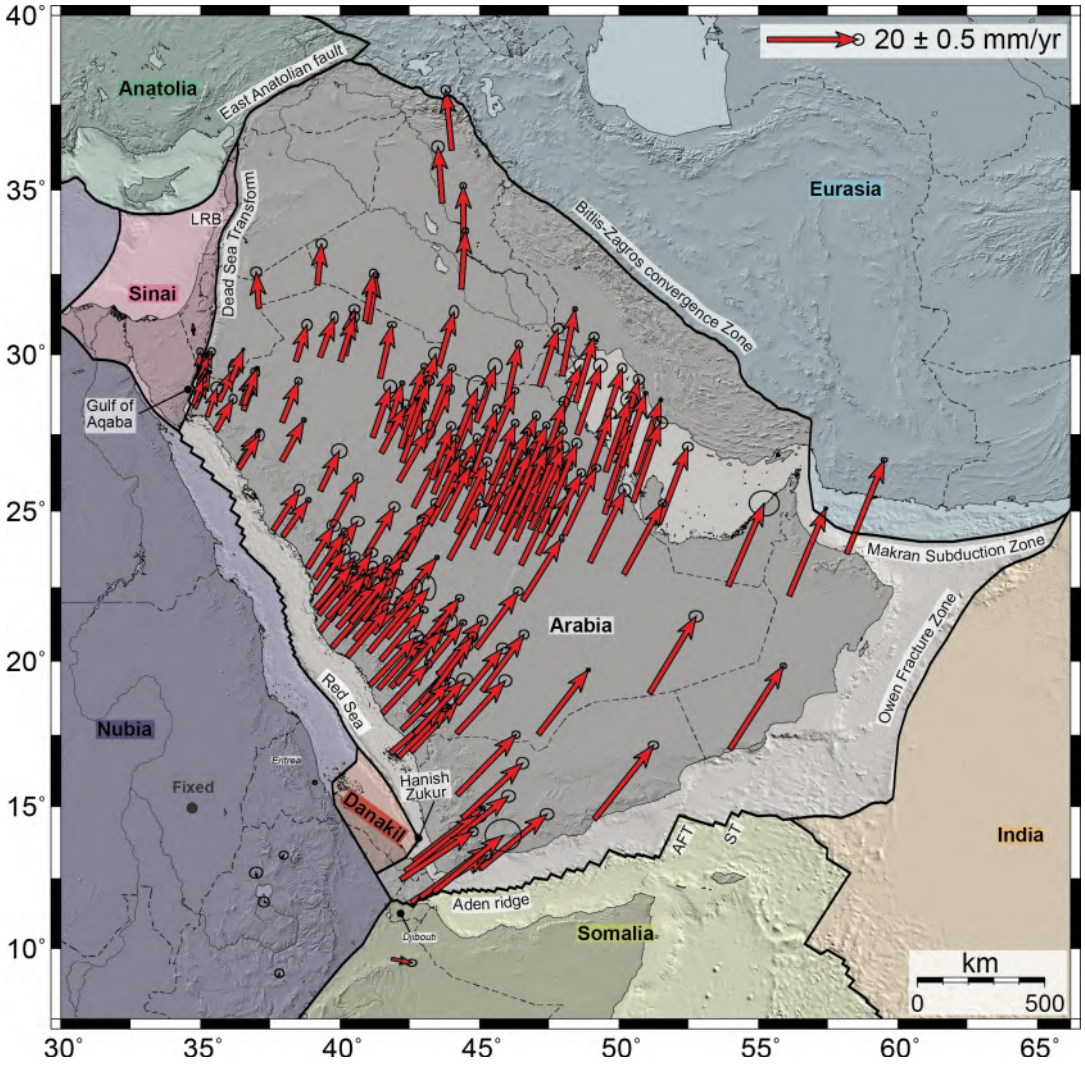

Figure 2. Horizontal GNSS velocities with 95% confidence ellipses rotated into a Nubian-fixed reference frame defined after the Altamimi et al. (2017) plate motion model. Black solid lines mark the simplified kinematic block model derived from the plate boundaries in Figure 1. Abbreviations: Lebanon restraining bend (LRB); Alula-Fartak (AFT), Socotra-Hadbeen (ST) transform fault. Background hillshaded topography and bathymetry are as in Figure 1.

GNSS velocities in the southernmost Red Sea, i.e., north of the western part of the Aden ridge along the Arabia-Somalia plate boundary confirm the full transfer of the Nubian-Arabian relative extension into Afar (Vigny et al., 2006; Doubre et al., 2017, Fig. 2). Their present-day motions are well described by the Nubian-Arabian angular velocities, indicating that the area in southern Eritrea and northern Djibouti currently represents a part of the Arabian plate (Barberi & Varet, 1977; Courtillot, 1982; Viltres et al., 2020, Fig. 1).

3.2 Kinematic model

The estimated angular velocity for the Arabian plate relative to the ITRF14 reference frame is consistent with counterclockwise rotation around an Euler pole located at 50.93±0.15°N, 353.91±0.25°E at a rate of 0.524±0.001°/Ma (Table 1). Our new estimate is within the 2-sigma uncertainties of the Altamimi et al. (2017) angular velocity, but significantly different from the Kreemer et al. (2014) results. The difference likely derives from the low number and distribution of GNSS stations used in the latter study, i.e., only 5 stations in the ESE part of the plate, including two redundant locations (See Table S1 in Kreemer et al., 2014, for details). The WRMS for the 168 sites used in the Arabian plate realization is 0.48 mm/yr, marginally better than the 0.60 mm/yr for 21, and 0.56 mm/yr for 5 GNSS sites used by ArRajehi et al. (2010) and Altamimi et al. (2017), respectively.

Our angular velocity estimates predict counterclockwise rotation of Arabia relative to the Nubian plate around an Euler pole located at 31.61±0.24°N, 24.22±0.31°E at a rate of 0.387±0.002°/Ma. The resulting Euler pole locates within ~0.4 angular degrees, but rotates ~5% faster compared with the Euler poles in ArRajehi et al. (2010), Reilinger and McClusky (2011), and Altamimi et al. (2017). However, at the 2-sigma uncertainty level, the angular velocities are indistinguishable. As expected from the previous results, we find significant discrepancies with Kreemer et al. (2014), which estimated Euler pole locates ~7 decimal degrees eastward and requires ~29% faster rotation rate.

The agreement between our results and the estimates from ArRajehi et al. (2010), Reilinger and McClusky (2011), and Altamimi et al. (2017) stands for the Arabian-Eurasian and Arabian-Somalian angular velocities of relative motion. However, our resulting Arabian-Indian angular velocity is significantly different from all the previous studies. The associated Euler pole locates up to ~43 and ~47 angular degrees southward and eastward, respectively, and requires a rotation rate up to ~3 times smaller relative to the former studies. Our predicted relative motions along this plate boundary are at the lower limit of the earlier estimates, but represent better the almost pure strike-slip tectonics of the Owen Fracture Zone (e.g., Rodriguez et al., 2019, Fig. 3).

Similar to the Arabian-Indian estimates, the Arabian-Sinai, and Arabian-Anatolian angular velocities reflect clear differences between recent studies addressing the present-day plate kinematics (e.g., ArRajehi et al., 2010; Reilinger & McClusky, 2011; Kreemer et al., 2014; Hamiel & Piatibratova, 2019; Gomez et al., 2020). In these cases, internal deformation (e.g., western Anatolian, Reilinger et al., 2006) combined with a limited number of GNSS stations, and the small size of the microplates (e.g., Sinai, ArRajehi et al., 2010) result in the variety of estimated angular velocities in the studies above. These elements may also

299 contribute in the ~2/4 and ~6/12 angular degree north and west shifts of the Danakil/Sinai
300 microplate instantaneous Euler pole relative to the long-term estimates for the last ~4.62
301 Ma by Schettino et al. (2016).

Table 1: GNSS-derived angular velocities and uncertainties.

Plate pair	(°)		(°/Ma)				Covariance matrix[a] (×10^{-6})					
	Lat.	Lon.	$\dot{\omega}$	$\dot{\omega}_x$	$\dot{\omega}_y$	$\dot{\omega}_z$	σ_{xx}	σ_{yy}	σ_{zz}	σ_{xy}	σ_{xz}	σ_{yz}
AR-ITRF14	50.93	353.91	0.524	0.3284	-0.0350	0.4068	1.76	1.59	0.72	1.63	1.07	1.02
AR-NU	31.61	24.22	0.387	0.3010	0.1354	0.2031	3.12	2.24	1.56	1.71	1.11	0.93
AR-EU	27.56	17.74	0.417	0.3519	0.1126	0.1928	3.18	1.87	2.50	1.68	2.29	1.10
AR-IN	25.49	313.77	0.020	0.0124	-0.0129	0.0085	10.56	143.29	17.82	32.13	10.77	5.52
AR-SO	23.91	26.53	0.420	0.3440	0.1717	0.1704	23.75	29.40	4.89	24.02	-4.58	5.19
AR-DA	13.83	42.19	-2.474	-1.7797	-1.6130	-0.5915	2671	1992	321	230	924	798
AR-SI*	36.34	14.97	0.135	0.1055	0.0282	0.0803	15.13	1.21	32.49	-	-	-
AR-AN*	27.79	42.45	-0.824	-0.5279	-0.4828	-0.4096	-	-	-	-	-	-

Notes: The angular velocities above describe the rotation of the Arabian plate (AR) relative to the second listed plate and the ITRF14 (defined after Altamimi et al., 2017). The Arabian-ITRF14 angular velocities are constrained by 168 GNSS stations. The present-day motions relative to the neighboring tectonic plates are constrained by recent estimates of their angular velocities relative to the ITRF14 (Altamimi et al., 2017; DeMets et al., 2019; Hamiel & Piatibratova, 2019), except for the Danakil and Sinai microplates, which Euler vectors were reported relative to the ITFR08 (Viltres et al., 2020; Gomez et al., 2020). [a] Elements of the angular velocity covariance matrix have units of (°/Ma)^2. * Full covariance matrices were not possible to estimate from the provided information in the respective studies (see Section 2.2). Abbreviations: Nubian (NU), Eurasian (EU), Indian (IN), Somalian (SM) plate, and Danakil (DA), Sinai (SI), Anatolian (AN) microplate.

302 The updated velocity field rotated into an Arabian-fixed reference frame defined after
303 the angular velocities estimated in this study (Table 1) is shown in Figure 3. The residual
304 GNSS velocities within the Arabian plate interior fall within the 95% confidence interval
305 for most of the stations, confirming the coherent rotation of the plate at present. Some
306 exceptions to this are observed across the plate and will be described in Section 3.4. As
307 previously mentioned, the WRMS for the 168 sites used in the Arabian plate realization is
308 0.48 mm/yr, indicating that our single Euler vector explains well almost all the observed
309 station motions.

310 3.3 Relative motion at plate boundaries

311 In addition to GNSS residual velocities, Figure 3 shows the rate and direction of the
312 predicted current motions along the Arabian plate boundary (blue arrows). Following the
313 strategy described in McClusky et al. (2010), we estimated the relative motion (strike-
314 slip and normal components) along the Arabian plate boundary associated with our set of
315 Euler vectors. As from our kinematic model, free-slip and vertical faults are assumed, and

316 therefore, the effects of the dip angles and elastic strain accumulation are not accounted
317 for. Besides, our block configuration provides a simplified description of the plate boundary
318 zones, particularly for the Levant and Iran regions, where present-day motions suggest the
319 interaction of additional microplates (e.g., Carmel, Mt. Lebanon, Syrian Coast, Helmand,
320 Lut, and Central Iran blocks, Vernant et al., 2004; Gomez et al., 2020, Fig. 1) not considered
321 in this study.

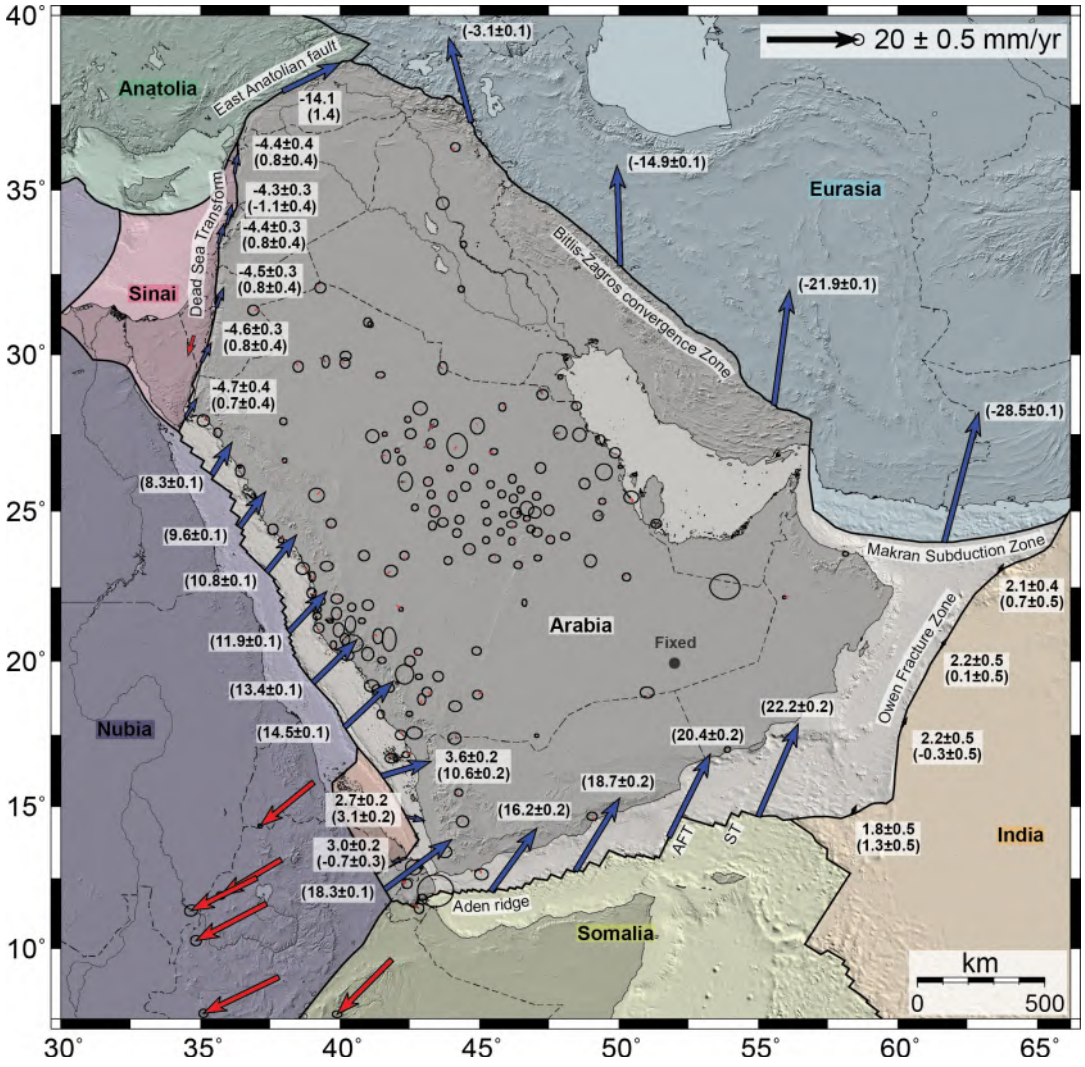

Figure 3. Observed GNSS velocities (red arrows), with 95% confidence ellipses, rotated into the Arabian-fixed reference from the kinematic block modeling results (Table 1). Blue arrows show predicted motions (east side with respect to the west side, or north with respect to south) at selected locations along the plate boundaries with the deduced normal and parallel components (mm/yr) being highlighted by white boxes. The numbers without parentheses (top) show the strike-slip component, with positive values being left-lateral sense of motion and the numbers in parentheses (bottom) show the normal component, with positive values being opening. Black solid lines mark the simplified kinematic block model derived from the plate boundaries in Figure 1. Background hillshaded topography and bathymetry are as in Figure 1.

The predicted velocities along the Arabian-Sinai plate boundary indicate primarily transtensional motions along the Dead Sea transform fault, consistent with 4.4-4.7 ± 0.3 mm/yr of left-lateral strike-slip, and ~0.8 ± 0.4 mm/yr of extension, except for the Lebanon restraining bend area (Fig. 1 and 3). Our estimates are in good agreement with recent studies in the region constrained by GNSS (e.g., Mahmoud et al., 2005; Reilinger et al., 2006; ArRajehi et al., 2010; Al Tarazi et al., 2011; Sadeh et al., 2012; Masson et al., 2015; Hamiel & Piatibratova, 2019; Gomez et al., 2020; Castro-Perdomo et al., 2021), InSAR (e.g., Li et al., 2021) and geological data (e.g., Klinger et al., 2000; Niemi et al., 2001; Ferry et al., 2007), particularly south of the Lebanon restraining bend (Fig. 1). At the center latitude of the Lebanon restraining bend (~34°N) where the block boundary turns eastward, our angular velocities predict average compressional motions of ~1.1 ± 0.4 mm/yr, consistent with the suggested shortening of the bend and in the Palmyride Mountains area (e.g., Kazmin, 2001; Alchalbi et al., 2010; ArRajehi et al., 2010, Fig. 3).

For the Arabian-Nubian and Arabian-Danakil plate pairs, the kinematic modeling indicates a gradual transfer of the Nubian-Arabian relative extension from the Red Sea into Afar (Fig. 1 and 3). From north to south, the extensional motions increase from ~7.2 ± 0.1 mm/yr at the latitude of the Nubian-Arabian-Sinai triple junction (~27.5°N) to ~15.0 ± 0.1 mm/yr at the Nubian-Arabian-Danakil triple junction (~17.0°N). From ~17.0°N to the Hanish-Zukur Islands group (~13.8°N) the Arabian-Nubian relative extension gradually dies out along the main axis of the southern Red Sea rift, simultaneously with a southward increase in differential motions on the western Danakil margin (Fig. 3). Going inland from the Hanish-Zukur Islands group, the predicted relative motions indicate primarily left-lateral strike-slip tectonics, with a fading extensional component as the block boundary cuts through Central Afar towards the inland axis of the southern Red Sea rift (Fig. 1 and 3). Here, the Arabian-Nubian predicted motions match the GNSS-derived velocities (0.8 mm/yr of WRMS for the 6 GNSS stations), indicating that the area is coherently moving with the Arabian plate at present (Fig. 3).

From west to east the Arabian-Somalian predicted opening motions range from ~15.2 ± 0.2 mm/yr in the Gulf of Tadjoura to ~22.9 ± 0.2 mm/yr near the Aden-Owen-Carlsberg triple junction (Fig. 1 and 3). The predicted extension rates are consistent with geodetic estimates of the relative plate motion by ArRajehi et al. (2010) and Altamimi et al. (2017). Likewise, the azimuth of the relative motion predicts the expected oblique extension along the Aden ridge, and pure strike-slip along the Alula-Fartak, and Socotra-Hadbeen transform faults (e.g., Leroy et al., 2004; D'Acremont et al., 2010; Ahmed et al., 2016, Fig. 1 and 3).

The azimuths of the predicted relative motion along the Arabian-Indian plates boundary

357 are in agreement with the right-lateral strike-slip motions prevailing over the last millions of

years along the OFZ (Fournier et al., 2008; Rodriguez et al., 2019). The model predictions indicate opening motions of ~0.7 ± 0.5 mm/yr and ~1.3 ± 0.5 mm/yr for the northern and southernmost extremities of the OFZ, respectively, consistent with the active normal faults associated with the Dalrymple Trough and the Beautemps-Beaupré pull-apart basin (Fournier et al., 2008; Rodriguez et al., 2014, Fig. 1 and 3). The kinematic modeling results predict mild compression at ~17.8°N, in contrast with former estimates (e.g., ArRajehi et al., 2010), but in line with the presence of restraining bends between ~16.5-20.3°N (Fournier et al., 2011). The average right-lateral strike-slip component for the OFZ (~2.2 ± 0.5 mm/yr) is at the lower limit of the MORVEL plate motion model (DeMets et al., 2010), and falls below former estimates constrained by GNSS (e.g., ~2.5-3.2 ± 0.5 mm/yr, ArRajehi et al., 2010) and multibeam and seismic data (e.g., ~4.2-5 mm/yr, Rodriguez et al., 2019).

For the northeastern Arabian plate boundary, our kinematic model shows a first-order description of the current regional-scale relative motions. A full description of the patterns of strain accumulation along this boundary requires updated constraints on the present-day motions of the Helmand, Lut, and central Iran blocks (e.g., Vernant et al., 2004; Reilinger et al., 2006; Khorrami et al., 2019). Using the Arabian-Eurasian plate boundary configuration and their associated angular velocity we estimate ~29.0 ± 0.1 mm/yr of roughly frontal shortening along the Makran subduction zone, and shortening motions decreasing towards northwest from ~22.0 ± 0.1 mm/yr to only ~3.0 ± 0.1 mm/yr along the Zagros collision zone (Fig. 1 and 3). Despite the omission of the central Iran block, the relative motion in the Zagros collision zone indicates the expected oblique convergence characterizing the complex stress regime of the area (Reilinger et al., 2006; Vernant & Chéry, 2006).

Our kinematic model predicts predominantly left-lateral strike-slip (~14 mm/yr) with a small opening component (<1.5 mm/yr) between the Arabian and the Anatolian plates (Fig. 3), similar to Reilinger et al. (2006) and Gomez et al. (2020). Compared with the former studies, our estimates result in a larger strike-slip, but a smaller normal component at this location. This suggests that a trade-off resulting from differences in the directions of relative block motion with respect to the local fault strikes is the main driver of the observed discrepancies.

3.4 Internal deformation

As discussed in Section 3.2, a single Euler pole can explain almost all the observed station motions within the Arabian plate interior (Fig. 3). Exceptions to this include 16 GNSS sites (9.5% of the stations) with residual velocities larger than 1.0 mm/yr. To test whether or not plate-wide internal motions could explain these residual velocities, we

392 included the parameters defining a uniform strain-rate tensor in our kinematic modeling.

The resulting uniform strain-rate tensor predicts 0.4 nanostrain/yr of ~N94°E oriented shortening, consistent with the magnitude of internal motions proposed by Vigny et al. (2006). The predicted internal motions fall, however, below the upper bound for stable plate interiors (e.g., Argus & Gordon, 1996; Gordon, 1998), confirming the broad-scale rigidity of the Arabian plate. Therefore, the major contributions to the observed differential motions are related either with locally straining areas that balance each other out within the plate (e.g., ArRajehi et al., 2010) or noise within our updated velocity field.

The results from our second analysis using the STIB method (Section 2.2) are shown in Figure 4. For visualization, the 0.5° grid estimates for the areal strain-rate (first invariant) were oversampled to 0.1° by means of the adjustable tension continuous curvature splines method (GMT5, Wessel et al., 2013). The resulting map shows effects from single isolated GNSS stations in the northern, and south-southeastern parts of the computational domain (Fig. 4). Thus, we focus our discussion mostly on the central part of the plate where the station coverage yields the highest baselines density.

At the plate-wide scale, the areal strain-rate map shows areas under extension neighbored by regions undertaking compressional motions. This is consistent with our previous result, as these competing differential motions almost entirely compensate within the plate, resulting in insignificant plate-wide strain rates. Still, several locally straining areas can be identified within the region of good spatial coverage of GNSS stations (numbered 1-9 in Fig. 4). Their distribution and strain orientation show no evidence of relation with intraplate tectonic structures, however, three of the extensional areas locate close to the Harrat Rahat volcanic field (4), the southern part of the Central Arabian graben system (6), and the Azraq graben (1), respectively. Instead, most of the areas are either located near agricultural fields (1-3, 5, 7, 9) or cities (6, 8). What is more, their spatial distribution correlates well with areas of known groundwater over-exploitation in Saudi Arabia, where 83-90% of the total water demand comes from agriculture (Abderrahman, 2001, Fig. 5). Besides, areas 6 and 8 locate near the cities of Riyadh and Al Hofuf, respectively, where significant ground subsidence resulting from rapid urbanization over units characterized by karst geomorphology have been identified (Amin & Bankher, 1997; Aljammaz et al., 2021).

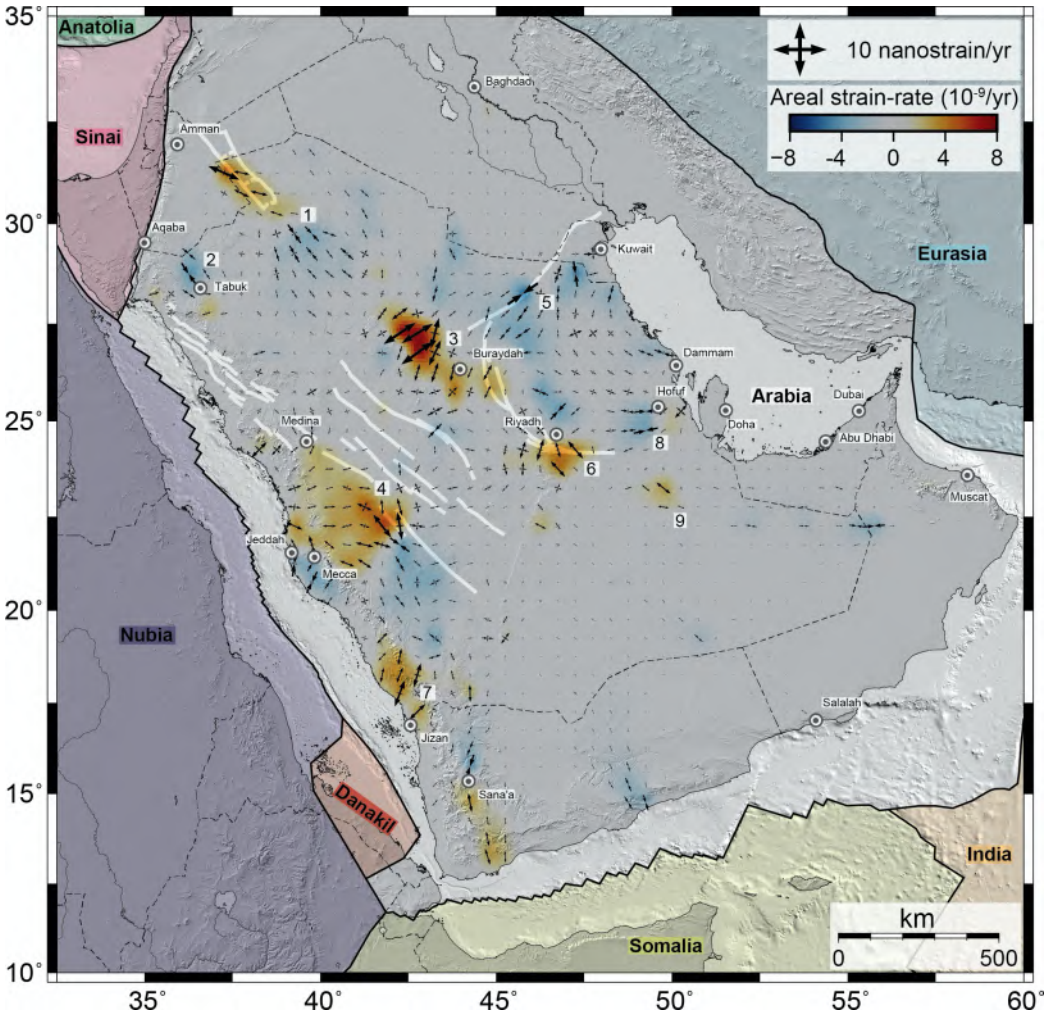

Figure 4. Principal horizontal strain rates and directions (black arrows) and areal strain-rate (first invariant, extension positive) estimated from the spatially-variable horizontal strain-rate tensor in Arabia. Black solid lines mark the simplified kinematic block model derived from the plate boundaries in Figure 1. Faint solid white lines and circled dots mark major intraplate tectonic structures shown in Fig. 1 and cities, respectively. Background hillshaded topography and bathymetry as in Figure 1.

4 Discussion

Our estimated Arabian-ITRF14 angular velocity implies consistency between recent derivations of the Arabian-Nubian-Eurasian relative plate motions (e.g., ArRajehi et al., 2010; Reilinger & McClusky, 2011; Altamimi et al., 2017), confirming the steady motion of the Arabian plate at present. The Arabian-Nubian Euler vector is also consistent within the 95% confidence interval with former estimates derived from combination of magnetic

anomaly profiles and earthquake slip vectors (e.g., Chu & Gordon, 1998; Schettino et al., 2016). This indicates that the present-day motions between the plates have remained unchanged since at least the time of the oldest magnetic lineation identified in the Red Sea (~4.62 Ma, Schettino et al., 2016). This time more than doubles when considering the agreement with the ArRajehi et al. (2010) and Reilinger and McClusky (2011) estimates, setting the time for steady motion of the Arabian relative to the Nubian and the Eurasian plates back to ~11 ± 2 and ~24 ± 4 Ma, respectively. We support this interpretation of steady motion between the plate triplet for the last ~11 ± 2 Ma, as the suggested 30 degrees northward shift of the Nubian-Eurasian Euler vector during recent geological times (e.g., Calais et al., 2003) would have become evident for at least one of the plate pairs, given the differences in number, geographic distribution, and observation time spans of the GNSS sites constraining the relative plate motion.

In addition to the Arabian-Somalian angular velocities reported by ArRajehi et al. (2010) and Reilinger and McClusky (2011), the updated estimates are consistent with the noise-reduced Euler vector obtained by Iaffaldano et al. (2014). Based on the plate paleo-positions during the last ~20 Ma (defined after Fournier et al., 2010) their study indicates that the plate pair relative motion remained stable since at least ~15 Ma. Likewise, the analysis of high-resolution sequences of finite rotations between the Indian-Somalian and Indian-Eurasian plates during the same time period indicates stationary poles of rotations for the two plate pairs since ~12.5 Ma (e.g., Iaffaldano et al., 2018; DeMets et al., 2019). Together, the results above imply the steady-state motion of the Arabian plate relative to the Nubian, Somalian, Indian, and Eurasian plates since at least the beginning of seafloor spreading along the full extent of the Red Sea ~13 Ma (Augustin et al., 2021).

The major discrepancies between our estimated angular velocities and recent estimates from ArRajehi et al. (2010) and Reilinger and McClusky (2011) are associated with the Arabian-Indian plate pair. Our new estimate predicts better the almost pure strike-slip tectonics of the OFZ, but seems to underestimate the magnitude of relative motion. At the predicted present-day slip rate (~2.2 mm/yr), our kinematic model yields an age for the formation of the OFZ of 4.5-5.4 Ma, consistent with the age range estimated by Fournier et al. (2008). However, recent analysis combining structural and stratigraphic studies indicate that the 10-12 km morphological offsets observed along the present location of the OFZ date only ~2.4 Ma, requiring dextral motions of 4.2-5 mm/yr along its entire length during this time (Rodriguez et al., 2019). A literal interpretation of the differences between the instantaneous and long-term predicted relative motion for the Arabian-Indian plate pair involves either increase in the Arabian-Eurasian and/or slowdown of the Indian-Eurasian convergence rate. We consider these scenarios rather unlikely taking into account the ap-

parent steady motion between the plate triplet during the last ~13 Ma (e.g., McQuarrie et al., 2003; ArRajehi et al., 2010; Reilinger & McClusky, 2011; Iaffaldano et al., 2014, 2018; DeMets et al., 2019). As stressed by DeMets et al. (2019), the angular velocity used to define the motion of the Indian plate in their study fails to reconcile the long-standing discrepancies between the predicted long-term and instantaneous India-Eurasia relative motion, despite being constrained by a larger number of GNSS stations compared with former estimates. Therefore, another direct interpretation of our results that needs to be tested is whether or not more than one Euler vector (additional blocks) are needed to fully explain the present-day motion of the Indian plate.

The predicted fault slip vectors for the Arabian-Anatolian and Arabian-Sinai plate boundaries are well represented by the focal mechanisms associated with the largest instrumental earthquakes nucleating along these boundaries, i.e., the 2020 Mw 6.7 Elazig, and the 1995 Mw 7.2 Nuweiba earthquake, respectively (U.S.G.S, 2021). The predominantly left-lateral strike-slip relative motions between the Arabian-Anatolian plate pair has been interpreted by Reilinger et al. (2006) as a result of lateral lithospheric transport out of the Arabia-Eurasian convergence zone associated with slab rollback forces along the Hellenic and Cyprus trenches (Fig. 1). As previously mentioned in Section 3.2, the updated Arabian-Sinai angular velocity simultaneously predicts well the predominant left-lateral strike-slip of the Dead Sea transform fault, while supporting the shortening motions around the Palmyride fold-thrust belt suggested by Alchalbi et al. (2010) and ArRajehi et al. (2010).

The Arabian-Danakil angular velocity predicts reducing opening motions to the southeast that vanish at the latitude of the Hanish Zukur Island group, consistent with the lack of seismic activity and oceanic crust beneath the Rea Sea south of ~13.8°N (e.g., Schettino et al., 2016; Augustin et al., 2021, Fig. 3), and the full transfer of the Nubia-Arabia relative extension into Afar (Vigny et al., 2006; McClusky et al., 2010; Doubre et al., 2017; Viltres et al., 2020). This result is further supported by the small WRMS for the 6 GNSS stations in central Afar (0.8 mm/yr, Section 3.2) that include 3 sites not considered in the angular velocity estimation because of their proximity the plate boundary (Fig. 3). Along the same line, our kinematic model results provide support for the addition of the southernmost part of Eritrea and northern Djibouti to the Arabian plate at present (Varet, 2018a; Viltres et al., 2020, Fig. 3).

The stable motion of the Arabian-Nubian plates since ~11 ± 2 Ma and the northward migration of the Danakil-Nubian Euler pole at ~5 Ma (e.g, McClusky et al., 2010; Reilinger & McClusky, 2011) implies a change of the Arabian-Danakil Euler pole at that time. Reilinger and McClusky (2011) associated this shift with the initiation of seafloor

spreading in the southern Red Sea based on oceanic crustal ages derived from magnetic anomalies (e.g., Cochran, 1983; Garfunkel & Beyth, 2006). However, recent results indicate that seafloor spreading along the entire length of the Red Sea dates back to ~13 Ma (Augustin et al., 2021), meaning that the Euler pole shift responds to a distinct geodynamic process in the area. We speculate that the Danakil-Nubia, and therefore, the Arabia-Danakil Euler pole shifts at ~5 Ma are related not to seafloor spreading in the southern Red Sea, but to the addition of the southernmost part of Eritrea and northern Djibouti as stabilized margins of the Arabian plate (Varet, 2018b, Fig. 3).

The horizontal strain-rate results suggest that the internal strains building up within the Arabian plate at present have mostly anthropogenic origins. Eight of about nine areas showing measurable strain rates are located either near areas known for groundwater over-exploitation or rapid urbanization, characterized by karst geomorphology (Amin & Bankher, 1997; López Valencia et al., 2020; Aljammaz et al., 2021; Müller Schmied et al., 2021, Figs. 4 - 6). Despite the spatial correlation between the deforming areas (1) and (6) with suggested structures belonging to the Azraq graben and the Central Arabian graben system we find the re-activation of these internal structures to be an unlikely driver of the observed strains. First, evidence of surface expression from the re-activation of these long-lived structures at present are missing (e.g, Konert et al., 2001; Faqira et al., 2009). In addition, the extensional strains estimated for some of these areas (i.e., 3, 6, 7, 9) are consistent with reports of shallow seismicity, opening cracks, and sinkholes in response to land subsidence mostly induced by water pumping (e.g., Youssef et al., 2014; Othman et al., 2018; Othman & Abotalib, 2019). Field observations show that extensional strains can develop in subsiding areas as a consequence of both vertical differential compaction and horizontal fluid flow in the subsurface (e.g., Sheng et al., 2003; Holzer & Galloway, 2005; Pacheco et al., 2006). Looking at the vertical velocity field (see Table S2 in the supplementary material for details), systematic upward motions are found in the Buraydah area, which may indicate some degree of aquifer recovery in the 2017-2019 period (Figs. 5 and 6). For the rest of the extensional straining zones (i.e., Riyadh, Jizan), the vertical velocities show downward motions. Thus, we suggest that differential compaction enhanced by well depths below 1000 meters (e.g., Othman & Abotalib, 2019) may provide the driving forces for the observed deformation.

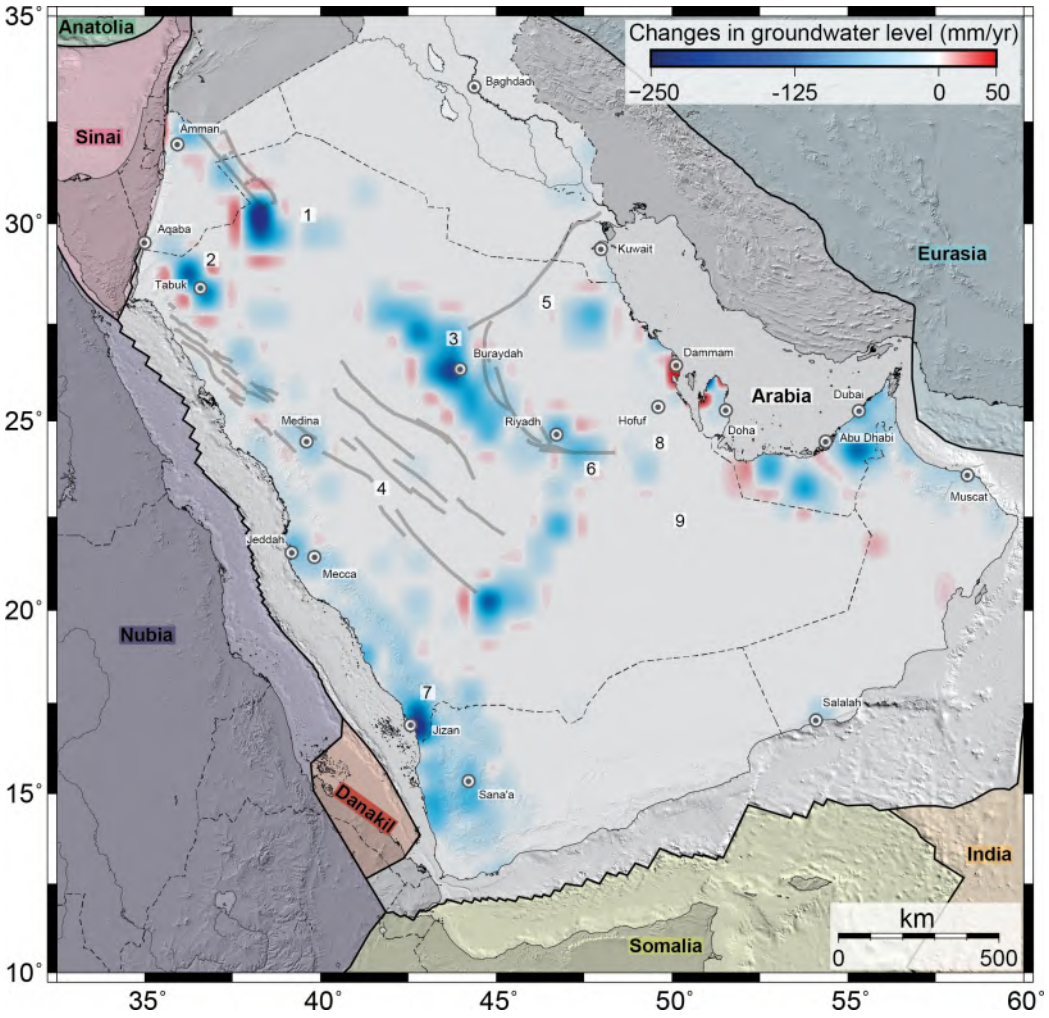

Figure 5. Changes in groundwater level for the time period 2000-2016 derived after the WaterGAP v2.2d model (Müller Schmied et al., 2021). Numbers 1-9 refer to areas showing significant local strain rates (see main text). Black solid lines mark the simplified kinematic block model derived from the plate boundaries in Figure 1. Faint solid grey lines and circled dots mark major intraplate tectonic structures shown in Fig. 1 and cities, respectively.

Even the straining area in central-west Saudi Arabia (4) is flanked by zones suggesting groundwater depletion, and therefore, the observed strains may include contributions from anthropogenic activity (Figs. 4 and 5). The horizontal strain-rate tensors for this area suggest roughly E-W oriented extension at the center and NW-SE extension at the sides. For the central part, the observed E-W oriented extension is consistent with the N-S direction of the proposed asthenospheric flow beneath the so-called MMN (Mecca-Madina-Nafud) line, well expressed by volcanic vent lineations in Harrat Rahat, Harrat Khaybar, and Harrat

Ithnayn, respectively (Camp & Roobol, 1992a; Pallister et al., 2010, Fig. 1). On the eastern side, where the strains are larger, the areal strain-rate map indicates clockwise rotation of the direction of extension, in line with the overall orientation of volcanic vents in Harrat Kishb, and Harrat Hadan volcanic fields, relative to the MMN line (Figs. 1 and 4). The maximum horizontal strains for this area reach ~5-6 nanostrain/yr within the Harrat Kishb and the northernmost Harrat Hadan volcanic fields, respectively (Fig. 1 and 4). This may indicate subsurface magmatic activity at present in an area that accounts for several volcanic eruptions during the last kiloyears, including at least one historical eruption in 1256 AD (Camp & Roobol, 1989; Downs et al., 2018).

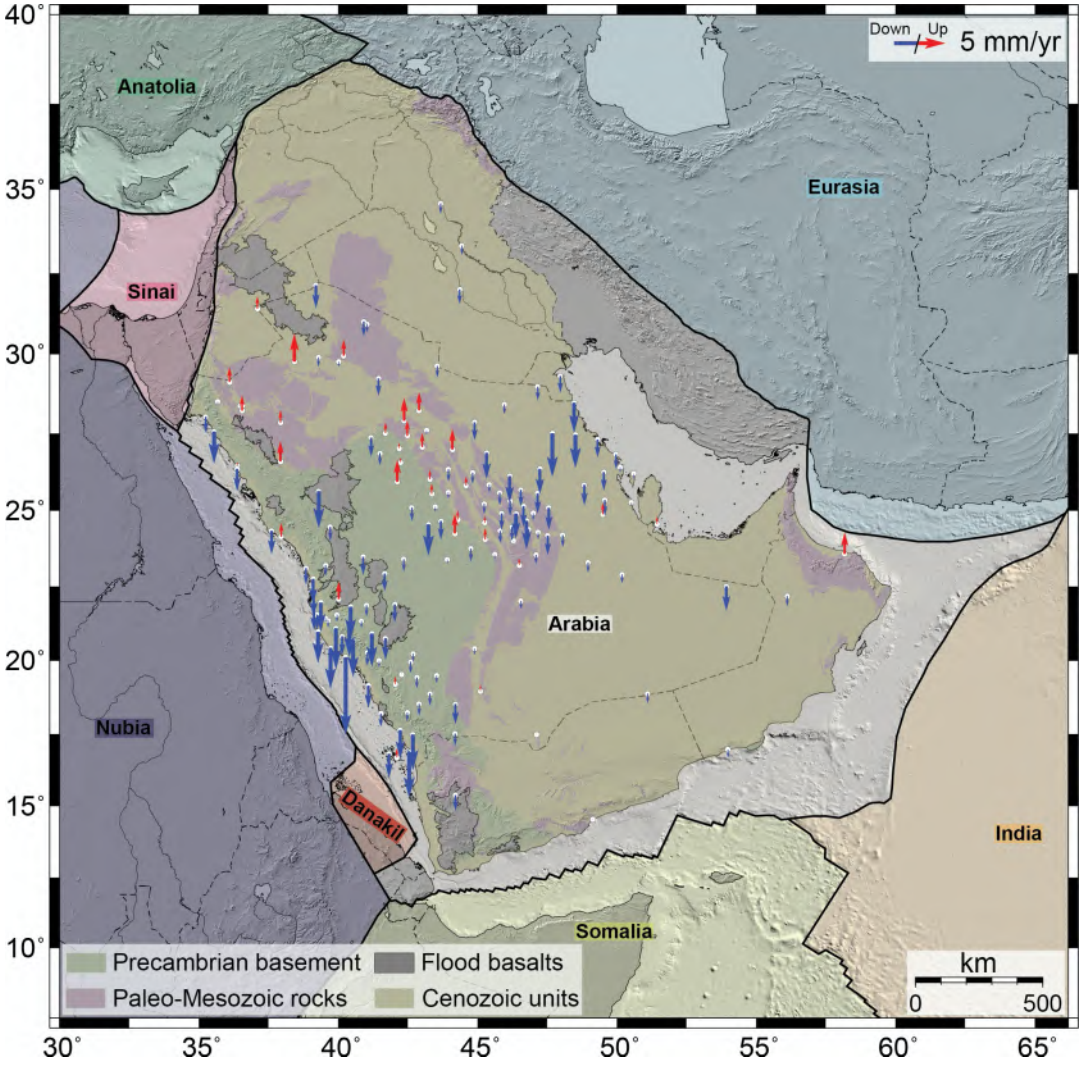

Figure 6. Vertical velocities for the continuous GNSS stations used in the block modeling presented in Section 3.2 and generalized age and rock type domains where the stations are located defined after Pollastro (1998).

Taken together, the results above show that the Arabian lithosphere is sufficiently strong to withstand large-scale forces associated with plate boundary processes (i.e., active continental collision and seafloor spreading on the northeastern and southwestern margins, respectively), gravitational potential energy differences, and basal drag (McClusky et al., 2000). This long-term stability of the plate likely results from a crust and lithosphere thickness combination that strengthens the plate interior and concentrates most of the deformation along its weaker margins (e.g., Jackson et al., 2021). Although very small, the estimated ~N94°E plate-wide shortening does not support for extensional forces associated with the Afar mantle plume and rifting along the Red Sea and the Gulf of Aden to be driving the Arabian plate into Eurasia as they will produce N-E oriented compression (e.g., Reilinger et al., 2006). Thus, we endorse the interpretations that the motion of Arabia is driven by far-field slab-pull forces resulting from the subduction of Afro-Arabian oceanic crust beneath Eurasia (Bellahsen et al., 2003).

5 Conclusions

In this study we analyzed GNSS measurements for 189 stations spanning between ~2.5 to ~17 years of continuous and survey mode observations to constrain the present-day motion and deformation of the Arabian plate. Our tightly constrained angular velocity for the Arabian-ITRF14 relative motion ($\dot{\omega}_x$ = 0.3284 ± 0.0013, $\dot{\omega}_y$ = -0.0350 ± 0.0013, and $\dot{\omega}_z$ = 0.4068 ± 0.0010 °/Ma) confirms that only one Euler vector is needed to explain the current station velocities. The kinematic modeling resulted in fault slip rates that are generally consistent with earlier estimates (e.g., ArRajehi et al., 2010; Reilinger & McClusky, 2011), except for the Arabian-Indian plate pair, for which slower right-lateral strike-slip motions are predicted. The small plate-wide internal strains (~0.4 nanostrains/yr) corroborate the large-scale rigidity of the Arabian plate, however, at a smaller scale, several areas of localized internal deformation can be identified. We postulate that differential compaction resulting from fossil groundwater over-exploitation and subsurface magmatic activity are the main drivers of the observed internal deformation. The Arabian lithosphere shows a remarkably long-term level of stability despite being affected by load forces associated with active continental collision in the northeast and breakup to the southwest.

6 Open Research

Global Navigation Satellite System (GNSS) daily files acquired within the Arabian plate and eastern Africa were accessed through the IGS (`https://cddis.nasa.gov/archive/gnss/data/daily`), Unavco (`https://www.unavco.org`, see King et al., 2019, for details), the King Abdullah University of Science and Technology

(see Jónsson, 2020, for detailes), the Saudi Arabia General Authority for Survey and Geospatial Information (https://ksacors.gcs.gov.sa), the French mobile network (https://gpsmob.resif.fr/donnees), the YOCMAL project (see Leroy, 2013, for details) and the King Abdulaziz City for Science and Technology (data available by request to the Geodesy and Navigation Center). The GNSS measurements were analyzed with the GAMIT/GLOBK (http://geoweb.mit.edu/gg/) software packages. Earthquake locations and focal mechanisms were downloaded from the International Seismological Centre (ISC, http://www.isc.ac.uk/iscbulletin/search/catalogue/, last accessed February 2022). Digital elevation model (DEM) and bathymetry data were downloaded from https://topex.ucsd.edu/ (last accessed July 2021). All plots in this article were produced using the Generic Mapping Tools version 5.4.5 (https://www.generic-mapping-tools.org) and the Python plotting library Matplotlib (https://matplotlib.org). The supplemental material for this article includes two tables with the horizontal and vertical components of the GNSS-derived velocity field, respectively.

Acknowledgments

This research was supported by King Abdullah University of Science and Technology (KAUST), under award number BAS/1/1353-01-01. We thank Professor Abdulkader M. Afifi (KAUST) for sharing his interpretation of the Arabian plate boundary, particularly along the Red Sea and Gulf of Aden regions. We also thank Frederique Rolandone (Sorbonne University) and Khaled Khanbari (Yemen Remote Sensing Center) for their contribution to data acquisition and supervision during the ANR-YOCMAL project in Yemen and Oman. We are grateful to the Saudi Arabia General Authority for Survey and Geospatial Information (GASGI) for providing most of the data used in this study. Likewise, we thank the various parties at King Abdulaziz City for Science and Technology (KACST) and the Saudi Geological Survey (SGS) for operating their GNSS networks through the years. We also thank Tectonics Associate Editor Paola Vannucchi and reviewers Andrea Walpersdorf and Gianluca Vignaroli for their comments and suggestions to an earlier version of this manuscript.

References

Abderrahman, W. A. (2001). Energy and water in arid developing countries: Saudi arabia, a case-study. *International Journal of Water Resources Development*, *17* (2), 247-255. doi: 10.1080/07900620120031306

Ahmed, A., Doubre, C., Leroy, S., Kassim, M., Keir, D., Abayazid, A., ... Al-Ganad, I.

(2016). Seafloor spreading event in western Gulf of Aden during the November 2010-March 2011 period captured by regional seismic networks: evidence for diking events and interactions with a nascent transform zone. *Geophysical Journal International* , *205* (2), 1244-1266. doi: 10.1093/gji/ggw068

Alchalbi, A., Daoud, M., Gomez, F., McClusky, S., Reilinger, R., Romeyeh, M. A., ... Barazangi, M. (2010). Crustal deformation in northwestern Arabia from GPS measurements in Syria: Slow slip rate along the northern Dead Sea Fault. *Geophysical Journal International* , *180* (1), 125-135. doi: 10.1111/j.1365-246X.2009.04431.x

Aldaajani, T., Furlong, K., & Malservisi, R. (2021). The rigidity of the wety/tern Arabian margin: extensional strain rate field from GPS networks. *Arabian Journal of Geosciences*, *14* (5), 393. doi: 10.1007/s12517-021-06751-x

Aldamegh, K. S., Hussein Moussa, H., Al-Arifi, S. N., Moustafa, S. S. R., & Moustafa, M. H. (2012). Focal mechanism of badr earthquake, saudia arabia of august 27, 2009. *Arabian Journal of Geosciences*, *5* (4), 599-606. doi: 10.1007/s12517-010-0200-8

Aljammaz, A., Sultan, M., Izadi, M., Abotalib, A. Z., Elhebiry, M. S., Emil, M. K., ... Becker, R. (2021). Land subsidence induced by rapid urbanization in arid environments: A remote sensing-based investigation. *Remote Sensing* , *13* (6). doi: 10.3390/rs13061109

Altamimi, Z., Métivier, L., Rebischung, P., Rouby, H., & Collilieux, X. (2017). ITRF2014 plate motion model. *Geophysical Journal International*, *209* (3), 1906-1912. doi: 10.1093/gji/ggx136

Al Tarazi, E., Abu Rajab, J., Gomez, F., Cochran, W., Jaafar, R., & Ferry, M. (2011). Gps measurements of near-field deformation along the southern dead sea fault system. *Geochemistry, Geophysics, Geosystems*, *12* (12). doi: 10.1029/2011GC003736

Amin, A. A., & Bankher, K. A. (1997). Karst hazard assessment of eastern saudi arabia. *Natural Hazards*, *15* (1), 21–30. doi: 10.1023/A:1007918623324

Argus, D. F., & Gordon, R. G. (1996). Tests of the rigid-plate hypothesis and bounds on intraplate deformation using geodetic data from very long baseline interferometry. *Journal of Geophysical Research: Solid Earth*, *101* (B6), 13555-13572.

ArRajehi, A., McClusky, S., Reilinger, R., & et al. (2010). Geodetic constraints on present-day motion of the Arabian Plate: Implications for Red Sea and Gulf of Aden rifting. *Tectonics*, *29* (3). doi: 10.1029/2009TC002482

Augustin, N., van der Zwan, F. M., Devey, C. W., & Brandsdóttir, B. (2021). 13 million years of seafloor spreading throughout the red sea basin. *Nature Communications*, *12* (1), 2427. doi: 10.1038/s41467-021-22586-2

Austermann, J., & Iaffaldano, G. (2013). The role of the zagros orogeny in slowing down arabia-eurasia convergence since 5 ma. *Tectonics*, *32* (3), 351-363.

Barberi, F., & Varet, J. (1977). Volcanism of afar: Small-scale plate tectonics implications. *GSA Bulletin*, *88*, 1251-1266. doi: 10.1130/0016-7606(1977)88〈1251:VOASPT〉2.0.CO;2

Bellahsen, N., Faccenna, C., Funiciello, F., Daniel, J., & Jolivet, L. (2003). Why did arabia separate from africa? insights from 3-d laboratory experiments. *Earth and Planetary Science Letters*, *216*(3), 365-381. doi: 10.1016/S0012-821X(03)00516-8

Bos, M. S., Fernandes, R. M. S., Williams, S. D. P., & Bastos, L. (2008). Fast error analysis of continuous gps observations. *Journal of Geodesy*, *82*(3), 157-166. doi: 10.1007/s00190-007-0165-x

Bos, M. S., Fernandes, R. M. S., Williams, S. D. P., & Bastos, L. (2013). Fast error analysis of continuous GNSS observations with missing data. *Journal of Geodesy*, *87*(4), 351-360. doi: 10.1007/s00190-012-0605-0

Bosworth, W., Huchon, P., & McClay, K. (2005). The red sea and gulf of aden basins. *Journal of African Earth Sciences*, *43*(1), 334-378. doi: 10.1016/j.jafrearsci.2005.07.020

Bosworth, W., Taviani, M., & Rasul, N. M. A. (2019). Neotectonics of the red sea, gulf of suez and gulf of aqaba. In I. C. Rasul Najeeb M.A.and Stewart (Ed.), *Geological setting, palaeoenvironment and archaeology of the red sea* (p. 11-35). Cham: Springer International Publishing. doi: 10.1007/978-3-319-99408-6_2

Calais, E., DeMets, C., & Nocquet, J.-M. (2003). Evidence for a post-3.16-ma change in nubia-eurasia-north america plate motions? *Earth and Planetary Science Letters*, *216*(1), 81-92. doi: 10.1016/S0012-821X(03)00482-5

Camp, V. E., & Roobol, M. J. (1989). The Arabian continental alkali basalt province: Part I. Evolution of Harrat Rahat, Kingdom of Saudi Arabia. *GSA Bulletin*, *101*(1), 71-95. doi: 10.1130/0016-7606(1989)101〈0071:TACABP〉2.3.CO;2

Camp, V. E., & Roobol, M. J. (1992a). Upwelling asthenosphere beneath western arabia and its regional implications. *Journal of Geophysical Research: Solid Earth*, *97*(B11), 15255-15271. doi: 10.1029/92JB00943

Camp, V. E., Roobol, M. J., & Hooper, P. R. (1992b). The Arabian continental alkali basalt province: Part III. Evolution of Harrat Kishb, Kingdom of Saudi Arabia. *GSA Bulletin*, *104*(4), 379-396. doi: 10.1130/0016-7606(1992)104〈0379:TACABP〉2.3.CO;2

Castro-Perdomo, N., Viltres, R., Masson, F., Klinger, Y., Liu, S., Dhahry, M., ... Jónsson, S. (2021). Interseismic deformation in the Gulf of Aqaba from GPS measurements. *Geophysical Journal International*, *228*(1), 477-492. doi: 10.1093/gji/ggab353

Chu, D., & Gordon, R. G. (1998). Current plate motions across the Red Sea. *Geophysical Journal International*, *135*(2), 313-328. doi: 10.1046/j.1365-246X.1998.00658.x

Cochran, J. R. (1983). A model for development of red sea. *Am. Assoc. Pet. Geol. Bull.*, *67*, 41-69. doi: 10.1144/GSL.SP.2006.259.01.04

Courtillot, V. (1982). Propagating rifts and continental breakup. *Tectonics*, *1* (3), 239-250. doi: 10.1029/TC001i003p00239

D'Acremont, E., Leroy, S., Maia, M., Gente, P., & Autin, J. (2010). Volcanism, jump and propagation on the Sheba ridge, eastern Gulf of Aden: segmentation evolution and implications for oceanic accretion processes. *Geophysical Journal International*, *180* (2), 535-551. doi: 10.1111/j.1365-246X.2009.04448.x

DeMets, C., Gordon, R. G., & Argus, D. F. (2010). Geologically current plate motions. *Geophysical Journal International*, *181* (1), 1-80. doi: 10.1111/j.1365-246X.2009.04491.x

DeMets, C., Merkouriev, S., & Jade, S. (2019, 11). High-resolution reconstructions and GPS estimates of India-Eurasia and India-Somalia plate motions: 20 Ma to the present. *Geophysical Journal International*, *220* (2), 1149-1171. doi: 10.1093/gji/ggz508

Doubre, C., Déprez, A., Masson, F., Socquet, A., Lewi, E., Grandin, R., ... Wright, T. (2017). Current deformation in Central Afar and triple junction kinematics deduced from GPS and InSAR measurements. *Geophysical Journal International*, *208* (2), 936-953. doi: 10.1093/gji/ggw434

Downs, D. T., Stelten, M. E., Champion, D. E., Dietterich, H. R., Nawab, Z., Zahran, H., ... Shawali, J. (2018). Volcanic history of the northernmost part of the Harrat Rahat volcanic field, Saudi Arabia. *Geosphere*, *14* (3), 1253-1282. doi: 10.1130/GES01625.1

Faqira, M., Rademakers, M., & Afifi, A. M. (2009). New insights into the Hercynian Orogeny, and their implications for the Paleozoic Hydrocarbon System in the Arabian Plate. *GeoArabia*, *14* (3), 199-228. doi: 10.2113/geoarabia1403199

Ferry, M., Meghraoui, M., Karaki, N. A., Al-Taj, M., Amoush, H., Al-Dhaisat, S., & Barjous, M. (2007). A 48-kyr-long slip rate history for the jordan valley segment of the dead sea fault. *Earth and Planetary Science Letters*, *260* (3), 394-406. doi: 10.1016/j.epsl.2007.05.049

Floyd, M. A., Billiris, H., Paradissis, D., Veis, G., Avallone, A., Briole, P., ... England, P. C. (2010). A new velocity field for greece: Implications for the kinematics and dynamics of the aegean. *Journal of Geophysical Research: Solid Earth*, *115* (B10). doi: 10.1029/2009JB007040

Fournier, M., Chamot-Rooke, N., Petit, C., Fabbri, O., Huchon, P., Maillot, B., & Lepvrier, C. (2008). In situ evidence for dextral active motion at the ArabiaIndia plate boundary. *Nature Geoscience*, *1* (1), 54-58.

Fournier, M., Chamot-Rooke, N., Petit, C., Huchon, P., Al-Kathiri, A., Audin, L., ... Merkouriev, S. (2010). Arabia-somalia plate kinematics, evolution of the aden-owen-

carlsberg triple junction, and opening of the gulf of aden. *Journal of Geophysical Research: Solid Earth*, *115* (B4).

Fournier, M., Chamot-Rooke, N., Rodriguez, M., Huchon, P., Petit, C., Beslier, M., & Zaragosi, S. (2011). Owen fracture zone: The arabia-india plate boundary unveiled. *Earth and Planetary Science Letters*, *302* (1), 247-252. doi: https://doi.org/10.1016/j.epsl.2010.12.027

Garfunkel, Z., & Beyth, M. (2006). Constraints on the structural development of afar imposed by the kinematics of the major surrounding plates. *Geological Society, London, Special Publications*, *259* (1), 23-42. doi: 10.1144/GSL.SP.2006.259.01.04

Gomez, F., Cochran, W. J., Yassminh, R., Jaafar, R., Reilinger, R., Floyd, M., ... Barazangi, M. (2020). Fragmentation of the Sinai Plate indicated by spatial variation in present-day slip rate along the Dead Sea Fault System. *Geophysical Journal International*, *221* (3), 1913-1940. doi: 10.1093/gji/ggaa095

Gordon, R. G. (1998). THE PLATE TECTONIC APPROXIMATION: Plate Nonrigidity, Diffuse Plate Boundaries, and Global Plate Reconstructions. *Annual Review of Earth and Planetary Sciences*, *26* (1), 615-642. doi: 10.1146/annurev.earth.26.1.615

Hamiel, Y., & Piatibratova, O. (2019). Style and distribution of slip at the margin of a pull-apart structure: Geodetic investigation of the southern dead sea basin. *Journal of Geophysical Research: Solid Earth*, *124* (11), 12023-12033. doi: 10.1029/2019JB018456

Hancock, P. L., Kadhi, A. A., & Sha'at, N. A. (1984). Regional joint sets in the arabian platform as indicators of intraplate processes. *Tectonics*, *3*, 27-43.

Henrion, E., Masson, F., Doubre, C., Ulrich, P., & Meghraoui, M. (2020). Present-day deformation in the Upper Rhine Graben from GNSS data. *Geophysical Journal International*, *223* (1), 599-611. doi: 10.1093/gji/ggaa320

Herring, T. A., King, R. W., Floyd, M. A., & McClusky, S. C. (2018). Documentation for the gamit/globk gps analysis software, release 10.7. *Department of Earth, Atmospheric, and Planetary Sciences, Massachusetts Institute of Technology, Cambridge*.

Holzer, T. L., & Galloway, D. L. (2005). Impacts of land subsidence caused by withdrawal of underground fluids in the United States. In J. Ehlen, W. C. Haneberg, & R. A. Larson (Eds.), *Humans as geologic agents* (Vol. 16, p. 87-99). Geological Society of America. doi: 10.1130/2005.4016(08)

Iaffaldano, G., Davies, D. R., & DeMets, C. (2018). Indian ocean floor deformation induced by the reunion plume rather than the tibetan plateau. *Nature Geoscience*, *11* (5), 362-366. doi: 10.1038/s41561-018-0110-z

Iaffaldano, G., Hawkins, R., & Sambridge, M. (2014). Bayesian noise-reduction in Arabia/Somalia and Nubia/Arabia finite rotations since 20 Ma: Implications for Nubia/Somalia relative motion. *Geochemistry, Geophysics, Geosystems*, *15* (4), 845-854.

765 ISC. (2022). *International Seismological Centre (2022), On-line Bulletin (last accessed*
766 *February 2022).* doi: 10.31905/D808B830
767 Jackson, J., McKenzie, D., & Priestley, K. (2021). Relations between earthquake distri-
768 butions, geological history, tectonics and rheology on the continents. *Philosophical*
769 *Transactions of the Royal Society A: Mathematical, Physical and Engineering Sci-*
770 *ences*, *379* (2193), 20190412. doi: 10.1098/rsta.2019.0412
771 Jónsson, S. (2012). Tensile rock mass strength estimated using insar. *Geophysical Research*
772 *Letters*, *39* (21). doi: 10.1029/2012GL053309
773 Jónsson, S. (2020). *Southern saudi arabia and eritrea 2016-gps/gnss observations dataset.*
774 doi: 10.7283/DR9Z-PV96
775 Kazmin, V. G. (2001). The late paleozoic to cainozoic intraplate deformation in north arabia:
776 a responce to plate boundary-forces. *Stephan Mueller Special Publication Series*, *2* ,
777 123-138.
778 Khorrami, F., VERNANT, P., Masson, F., Nilfouroushan, F., Mousavi, Z., Nankali, H., ...
779 Alijanzade, M. (2019). An up-to-date crustal deformation map of Iran using integrated
780 campaign-mode and permanent GPS velocities. *Geophysical Journal International* ,
781 *217* (2), 832-843. doi: 10.1093/gji/ggz045
782 King, R., Floyd, M., Reilinger, R., & Bendick, R. (2019). *Gps velocity field (mit 2019.0)*
783 *for the east african rift system generated by king et al.* doi: 10.1594/IEDA/324785
784 Klinger, Y., Avouac, J. P., Abou Karaki, N., Dorbath, L., Bourles, D., & Reyss, J. L.
785 (2000). Slip rate on the Dead Sea transform fault in northern Araba valley (Jordan).
786 *Geophysical Journal International* , *142* (3), 755-768. doi: 10.1046/j.1365-246x.2000
787 .00165.x
788 Kogan, L., Fisseha, S., Bendick, R., Reilinger, R., McClusky, S., King, R., & Solomon, T.
789 (2012). Lithospheric strength and strain localization in continental extension from
790 observations of the east african rift. *Journal of Geophysical Research: Solid Earth*,
791 *117* (B3). doi: 10.1029/2011JB008516
792 Konert, G., Afifi, A. M., Al-Hajri, S. A., & Droste, H. J. (2001, 07). Paleozoic Stratigraphy
793 and Hydrocarbon Habitat of the Arabian Plate. *GeoArabia*, *6* (3), 407-442. doi:
794 10.2113/geoarabia0603407
795 Kreemer, C., Blewitt, G., & Klein, E. C. (2014). A geodetic plate motion and global
796 strain rate model. *Geochemistry, Geophysics, Geosystems*, *15* (10), 3849-3889. doi:
797 10.1002/2014GC005407
798 Leroy, S. (2013). *Young conjugate margins laboratory in the gulf of aden (yocmal) project,*
799 *anr 07-blan-135-02.*
800 Leroy, S., Gente, P., Fournier, M., D'Acremont, E., Patriat, P., Beslier, M.-O., Huchon,
801 P. (2004). From rifting to spreading in the eastern gulf of aden: a geophysical survey

of a young oceanic basin from margin to margin. *Terra Nova*, *16*(4), 185-192. doi: 10.1111/j.1365-3121.2004.00550.x

Leroy, S., Razin, P., Autin, J., Bache, F., d'Acremont, E., Watremez, L., . . . Al Lazki, A. (2012). From rifting to oceanic spreading in the gulf of aden: a synthesis. *Arabian Journal of Geosciences*, *5*(5), 859-901. doi: 10.1007/s12517-011-0475-4

Li, X., Jnsson, S., & Cao, Y. (2021). Interseismic deformation from sentinel-1 burst-overlap interferometry: Application to the southern dead sea fault. *Geophysical Research Letters*, *n/a*(n/a), e2021GL093481. doi: 10.1029/2021GL093481

Lim, J.-A., Chang, S.-J., Mai, P. M., & Zahran, H. (2020). Asthenospheric Flow of Plume Material Beneath Arabia Inferred From S Wave Traveltime Tomography. *Journal of Geophysical Research: Solid Earth*, *125*(8), e2020JB019668. doi: 10.1029/2020JB019668

López Valencia, O. M., Johansen, K., Aragón Solorio, B. J. L., Li, T., Houborg, R., Malbeteau, Y., . . . McCabe, M. F. (2020). Mapping groundwater abstractions from irrigated agriculture: big data, inverse modeling, and a satellite–model fusion approach. *Hydrology and Earth System Sciences*, *24*(11), 5251-5277. doi: 10.5194/hess-24-5251-2020

Mahmoud, S., Reilinger, R., McClusky, S., Vernant, P., & Tealeb, A. (2005). Gps evidence for northward motion of the sinai block: Implications for e. mediterranean tectonics. *Earth and Planetary Science Letters*, *238*(1), 217-224. doi: 10.1016/j.epsl.2005.06.063

Masson, F., Hamiel, Y., Agnon, A., Klinger, Y., & Deprez, A. (2015). Variable behavior of the dead sea fault along the southern arava segment from gps measurements. *Comptes Rendus Geoscience*, *347*(4), 161-169. doi: 10.1016/j.crte.2014.11.001

Masson, F., Lehujeur, M., Ziegler, Y., & Doubre, C. (2014). Strain rate tensor in Iran from a new GPS velocity field. *Geophysical Journal International*, *197*(1), 10-21. doi: 10.1093/gji/ggt509

McCaffrey, R. (1995). Defnode users' guide. *Rensselaer Polytech. Inst.*.

McCaffrey, R. (2002). Crustal block rotations and plate coupling. In *Plate boundary zones* (p. 101-122). American Geophysical Union (AGU). doi: 10.1029/GD030p0101

McCaffrey, R. (2009). Time-dependent inversion of three-component continuous gps for steady and transient sources in northern cascadia. *Geophysical Research Letters*, *36*(7). doi: 10.1029/2008GL036784

McClusky, S., Balassanian, S., Barka, A., Demir, C., Ergintav, S., Georgiev, I., . . . Veis, G. (2000). Global positioning system constraints on plate kinematics and dynamics in the eastern mediterranean and caucasus. *Journal of Geophysical Research: Solid Earth*, *105*(B3), 5695-5719. doi: 10.1029/1999JB900351

McClusky, S., Reilinger, R., Mahmoud, S., Ben Sari, D., & Tealeb, A. (2003). GPS con-

straints on Africa (Nubia) and Arabia plate motions. *Geophysical Journal International*, *155* (1), 126-138. doi: 10.1046/j.1365-246X.2003.02023.x

McClusky, S., Reilinger, R., Ogubazghi, G., Amleson, A., Healeb, B., Vernant, P., ... Kogan, L. (2010). Kinematics of the southern red sea-afar triple junction and implications for plate dynamics. *Geophysical Research Letters*, *37* (5). doi: 10.1029/2009GL041127

McQuarrie, N., Stock, J. M., Verdel, C., & Wernicke, B. P. (2003). Cenozoic evolution of neotethys and implications for the causes of plate motions. *Geophysical Research Letters*, *30* (20).

Müller Schmied, H., Cáceres, D., Eisner, S., Flörke, M., Herbert, C., Niemann, C., ... Döll, P. (2021). The global water resources and use model watergap v2.2d: model description and evaluation. *Geoscientific Model Development*, *14* (2), 1037-1079. doi: 10.5194/gmd-14-1037-2021

Niemi, T. M., Zhang, H., Atallah, M., & Harrison, J. B. J. (2001). Late Pleistocene and Holocene slip rate of the Northern Wadi Araba fault, Dead Sea Transform, Jordan. *Journal of Seismology*, *5* (3), 449-474. doi: 10.1023/A:1011487912054

Othman, A., & Abotalib, A. Z. (2019). Land subsidence triggered by groundwater withdrawal under hyper-arid conditions: case study from central saudi arabia. *Environmental Earth Sciences*, *78* (7), 243. doi: 10.1007/s12665-019-8254-8

Othman, A., Sultan, M., Becker, R., Alsefry, S., Alharbi, T., Gebremichael, E., ... Abdelmohsen, K. (2018). Use of geophysical and remote sensing data for assessment of aquifer depletion and related land deformation. *Surveys in Geophysics*, *39* (3), 543-566. doi: 10.1007/s10712-017-9458-7

Pacheco, J., Arzate, J., Rojas, E., Arroyo, M., Yutsis, V., & Ochoa, G. (2006). Delimitation of ground failure zones due to land subsidence using gravity data and finite element modeling in the querétaro valley, méxico. *Engineering Geology*, *84*, 143-160.

Pallister, J. S., McCausland, W. A., Jónsson, S., Lu, Z., Zahran, H. M., Hadidy, S. E., ... Moufti, M. R. H. (2010). Broad accommodation of rift-related extension recorded by dyke intrusion in saudi arabia. *Nature Geoscience*, *3* (10), 705-712. doi: 10.1038/ngeo966

Pollastro, R. M. (1998). *Bedrock geology of the arabian peninsula and selected adjacent areas (geo2bg).* https://catalog.data.gov/dataset/bedrock-geology-of-the-arabian-peninsula-and-selected-adjacent-areas-geo2bg.

Reilinger, R., & McClusky, S. (2011). Nubia-Arabia-Eurasia plate motions and the dynamics of Mediterranean and Middle East tectonics. *Geophysical Journal International*, *186* (3), 971-979. doi: 10.1111/j.1365-246X.2011.05133.x

Reilinger, R., McClusky, S., & ArRajehi, A. (2015). Geodetic constraints on the geodynamic evolution of the red sea. In N. M. Rasul & I. C. Stewart (Eds.), *The red sea: The*

formation, morphology, oceanography and environment of a young ocean basin (p. 135-149). Berlin, Heidelberg: Springer Berlin Heidelberg. doi: 10.1007/978-3-662-45201-1_7

Reilinger, R., McClusky, S., Vernant, P., Lawrence, S., Ergintav, S., Cakmak, R., Karam, G. (2006). Gps constraints on continental deformation in the africa-arabia-eurasia continental collision zone and implications for the dynamics of plate interactions. *Journal of Geophysical Research: Solid Earth*, *111* (B5). doi: 10.1029/2005JB004051

Ribot, M., Klinger, Y., Jónsson, S., Avsar, U., Pons-Branchu, E., Matrau, R., & Mallon, F. L. (2021). Active faults' geometry in the gulf of aqaba, southern dead sea fault, illuminated by multibeam bathymetric data. *Tectonics*, *40* (4), e2020TC006443. doi: 10.1029/2020TC006443

Robinet, J., Razin, P., Serra-Kiel, J., Gallardo-Garcia, A., Leroy, S., Roger, J., & Grelaud, C. (2013). The paleogene pre-rift to syn-rift succession in the dhofar margin (northeastern gulf of aden): Stratigraphy and depositional environments. *Tectonophysics*, *607* , 1-16. doi: 10.1016/j.tecto.2013.04.017

Rodriguez, M., Chamot-Rooke, N., Huchon, P., Fournier, M., Lallemant, S., Delescluse, M., Mouchot, N. (2014). Tectonics of the Dalrymple Trough and uplift of the Murray Ridge (NW Indian Ocean). *Tectonophysics*, *636* , 1-17. doi: 10.1016/j.tecto.2014.08.001

Rodriguez, M., Huchon, P., Chamot-Rooke, N., Fournier, M., & Delescluse, M. (2019). Structural reorganization of the India-Arabia strike-slip plate boundary (Owen Fracture Zone; NW Indian Ocean) 2.4 million years ago. In J. C. Duarte (Ed.), *Transform Plate Boundaries and Fracture Zones* (p. 146-155). Elsevier. doi: 10.1016/B978-0-12-812064-4.00007-4

Sadeh, M., Hamiel, Y., Ziv, A., Bock, Y., Fang, P., & Wdowinski, S. (2012). Crustal deformation along the dead sea transform and the carmel fault inferred from 12 years of gps measurements. *Journal of Geophysical Research: Solid Earth*, *117* (B8). doi: 10.1029/2012JB009241

Schettino, A., Macchiavelli, C., Pierantoni, P. P., Zanoni, D., & Rasul, N. (2016). Recent kinematics of the tectonic plates surrounding the Red Sea and Gulf of Aden. *Geophysical Journal International*, *207* (1), 457-480. doi: 10.1093/gji/ggw280

Sheng, Z., Helm, D. C., & Li, J. (2003). Mechanisms of Earth Fissuring Caused by Groundwater Withdrawal. *Environmental and Engineering Geoscience*, *9* (4), 351-362.

Spakman, W., & Nyst, M. (2002). Inversion of relative motion data for estimates of the velocity gradient field and fault slip. *Earth and Planetary Science Letters*, *203* (1), 577-591. doi: 10.1016/S0012-821X(02)00844-0

Stern, R. J., & Johnson, P. (2010). Continental lithosphere of the arabian plate: A geologic,

petrologic, and geophysical synthesis. *Earth-Science Reviews*, *101* (1), 29-67. doi: 10.1016/j.earscirev.2010.01.002

Trippanera, D., Ruch, J., Passone, L., & Jónsson, S. (2019). Structural Mapping of Dike-Induced Faulting in Harrat Lunayyir (Saudi Arabia) by Using High Resolution Drone Imagery. *Frontiers in Earth Science*, *7*. doi: 10.3389/feart.2019.00168

U.S.G.S. (2021). *Earthquake Catalogue.* https://earthquake.usgs.gov/earthquakes/search/.

Varet, J. (2018a). Transverse volcanic alignments along afar margins. In *Geology of Afar (East Africa)* (p. 241-251). Cham: Springer International Publishing. doi: 10.1007/978-3-319-60865-5 9 _

Varet, J. (2018b). Afar, a hot-spot for earth's geodynamics studies. In *Geology of afar (east africa)* (p. 285-293). Cham: Springer International Publishing. doi: 10.1007/978-3-319-60865-5 11_

Vernant, P., & Chéry, J. (2006). Mechanical modelling of oblique convergence in the zagros, iran. *Geophysical Journal International*, *165* (3), 991-1002. doi: 10.1111/j.1365-246X.2006.02900.x

Vernant, P., Nilforoushan, F., Hatzfeld, D., Abbassi, M. R., Vigny, C., Masson, F., Chry, J. (2004, 04). Present-day crustal deformation and plate kinematics in the Middle East constrained by GPS measurements in Iran and northern Oman. *Geophysical Journal International*, *157* (1), 381-398. doi: 10.1111/j.1365-246X.2004.02222.x

Vigny, C., Huchon, P., Ruegg, J.-C., Khanbari, K., & Asfaw, L. M. (2006). Confirmation of arabia plate slow motion by new gps data in yemen. *Journal of Geophysical Research: Solid Earth*, *111* (B2). doi: 10.1029/2004JB003229

Viltres, R., Jónsson, S., Ruch, J., Doubre, C., Reilinger, R., Floyd, M., & Ogubazghi, G. (2020). Kinematics and deformation of the southern Red Sea region from GPS observations. *Geophysical Journal International*, *221* (3), 2143-2154. doi: 10.1093/gji/ggaa109

Wessel, P., W. H. F., S., R., S., J., L., & Wobbe, F. (2013). Generic mapping tools: Improved version released. *EOS Trans. AGU*, *94* (45), 409-410.

Williams, S. D. P. (2003). The effect of coloured noise on the uncertainties of rates estimated from geodetic time series. *Journal of Geodesy*, *76* (9), 483–494. doi: 10.1007/s00190-002-0283-4

Williams, S. D. P. (2008). CATS: GPS coordinate time series analysis software. *GPS Solutions*, *12* (2), 147–153. doi: 10.1007/s10291-007-0086-4

Wu, Y., Jiang, Z., Yang, G., Wei, W., & Liu, X. (2011). Comparison of GPS strain rate computing methods and their reliability. *Geophysical Journal International* , *185* (2), 703-717. doi: 10.1111/j.1365-246X.2011.04976.x

Xu, W., Dutta, R., & Jónsson, S. (2015b). Identifying Active Faults by Improving Earth-

quake Locations with InSAR Data and Bayesian Estimation: The 2004 Tabuk (Saudi Arabia) Earthquak e Sequence. *Bulletin of the Seismological Society of America*, *105* (2A), 765-775. doi: 10.1785/0120140289

Xu, W., Jónsson, S., Corbi, F., & Rivalta, E. (2016). Graben formation and dike arrest during the 2009 harrat lunayyir dike intrusion in saudi arabia: Insights from insar, stress calculations and analog experiments. *Journal of Geophysical Research: Solid Earth*, *121* (4), 2837-2851. doi: 10.1002/2015JB012505

Youssef, A. M., Sabtan, A. A., Maerz, N. H., & Zabramawi, Y. A. (2014). Earth Fissures in Wadi Najran, Kingdom of Saudi Arabia. *Natural Hazards*, *71* (3), 2013-2027. doi: 10.1007/s11069-013-0991-5